INCORPORATING THE EFFECTS OF TURBULENCE LENGTH SCALE IN TURBULENCE AND TRANSITION MODELS FOR TURBOMACHINERY FLOWS

C. Bode[1], D. Kožulović[1], M. Franke[2], K. Westhäuser[2]

[1]Technische Universität Braunschweig
Institut für Strömungsmechanik
Bienroder Weg 3, D-38106 Braunschweig
Phone: +49 531 391 2976, Fax: +49 531 391 5952
chr.bode@tu-braunschweig.de

[2]MTU Aero Engines GmbH
Dachauerstr. 665, D-80995 München

ABSTRACT

An approach for the estimation of the turbulence length scale at the inflow boundary is presented. This estimation yields reasonable turbulence decay, supporting the transition model in accurately predicting the laminar-turbulent transition location and development. As an additional element of the approach, the sensitivity of the turbulence model to free-stream values is suppressed by limiting the eddy viscosity in non-viscous regions. The method is implemented in DLR's turbomachinery flow solver TRACE in the framework of the k-ω turbulence model by Wilcox and the γ-Re_θ transition model by Langtry and Menter. The improved model is applied to the ERCOFTAC T3 testcases, T106A turbine and HPA 17/06 compressor cascade and is compared to experimental data.

NOMENCLATURE

c_p	pressure coefficient, $(p_W - p_2)/(p_{t1} - p_2)$
k	turbulent kinetic energy, $(\overline{u'^2} + \overline{v'^2} + \overline{w'^2})/2$
l	chord length
l_T	turbulent length scale
M	Mach number, U/a
M_{is}	isentropic Mach number
p	static pressure
p_t	total pressure
Re	Reynolds number, $U\,l/\nu$
Tu	turbulence level (%)
y^+	dimensionless wall distance, $u_\tau\,y/\nu$
x, y, z	Cartesian coordinates
b_v	new CFD flow field variable blend viscous
b	wire thickness of the turbulence grid

Greek

β	inlet angle
ζ	loss coefficient
κ	isentropic exponent, $\kappa = 1,4$
θ	momentum thickness, $\int_0^\delta \frac{\rho U}{\rho_E U_E}\left(1 - \frac{U}{U_E}\right) dy$
ρ	density
ω	specific turbulent dissipation rate
γ	intermittency of transition model
μ	molecular viscosity
μ_t	eddy viscosity

Subscripts

is	isentropic
t	total
th	theoretical
0	Inlet: boundary condition
1	Inlet: upstream of the blade
2	Outlet: downstream of the blade
sep	separation
eff	effective
FS	free stream
w	wall
∞	outer flow
T	turbine
V	compressor

Abbreviations

CFD	Computational Fluid Dynamics
DLR	German Aerospace Center
$TRACE$	Turbomachinery Research Aerodynamics Computational Environment

1 INTRODUCTION

Laminar-turbulent transition plays a significant role in the boundary layer development of modern highly-loaded low-pressure turbine (LPT) profiles, and to a smaller degree for compressor profiles. The significance is even accentuated due to the drop of Reynolds numbers at high flight altitudes, that means at cruise conditions. Some turbine profiles operate at Reynolds numbers as low as $Re_{2th} \leq 1 \cdot 10^5$, showing a large laminar boundary layer patch with subsequent separation and turbulent reattachment, cf. Mayle [1] and Hourmouziadis [2].

There exist many approaches for the prediction of laminar-turbulent transition. For turbomachinery flows, a combination of a RANS (Reynolds-averaged Navier-Stokes) turbulence model with a correlation-based transition model is widely spread. In this work, the combination of the k-ω turbulence model by Wilcox [3] and the γ-Re_θ transition model by Langtry and Menter [4] is applied.

The transition process is influenced by many parameters, e.g. turbulence intensity, Reynolds number, pressure gradient, etc. Most transition models capture this influence by taking the corresponding parameters into account, in one way or another. In the present framework, the influence of the turbulence length scale is also indirectly captured by the turbulence decay behaviour of the turbulence model. Depending on the prescribed turbulence length scale (l_T) at the inflow boundary, different dissipation rates will arise, with significantly altered decay of turbulence intensity. This leads to a shift in transition prediction, since the transition model is coupled to the turbulence intensity. Turbomachinery flows are very prone to this effect, due to high turbulence levels and corresponding sensitivity to dissipation rate (or length scale) prescription. As many experiments do not provide the turbulence length scale, the CFD users feel free to choose a value, often one that best fits the experimental data. Hence, a correlation for the estimation of the turbulence length scale is derived. This correlation reasonably fits various experimental data.

2 NUMERICAL METHOD

As an up-to-date numerical method, the parallel CFD-solver TRACE of DLR Köln has been applied, cf. Nürnberger [5], Kügeler [6], Marciniak [7] and Becker [8]. In this solver, the three-dimensional Reynolds-averaged Navier-Stokes equations are solved on multi-block meshes by a finite volume technique. The convective fluxes are discretized by the TVD upwind scheme of Roe [9] and the diffusive fluxes by a central differencing scheme. An implicit predictor-corrector time integration algorithm has been used for the steady simulations. The turbulence is modelled by the two-equation $k-\omega$ model of Wilcox [3], together with the Kato-Launder [10] fix for the stagnation point anomaly. Furthermore, non-reflecting boundary conditions by Saxer and Giles [11] have been applied to the inlet and outlet boundaries. The boundary layer transition has been modelled by the $\gamma - Re_\theta$ transport equation transition model after Langtry and Menter [4]. It evaluates the local flow features to model natural, bypass and separation induced transition. Only the wall distance formulation is non local. The transport equations for γ and $Re_{\theta t}$ are defined as followed:

(1)
$$\frac{\delta(\rho\gamma)}{\delta t} + \frac{\delta(\rho U_j \gamma)}{\delta x_j} = P_{\gamma 1} - E_{\gamma 1} + P_{\gamma 2} - E_{\gamma 2} + \frac{\delta}{\delta x_j}\left[\left(\mu + \frac{\mu_t}{\sigma_f}\right)\frac{\delta\gamma}{\delta x_j}\right]$$

(2)
$$\frac{\delta\left(\rho\tilde{Re}_{\theta t}\right)}{\delta t} + \frac{\delta\left(\rho U_j \tilde{Re}_{\theta t}\right)}{\delta x_j} = P_{\theta t} + \frac{\delta}{\delta x_j}\left[\sigma_{\theta t}(\mu + \mu_t)\frac{\delta\tilde{Re}_{\theta t}}{\delta x_j}\right]$$

The source terms P_γ and E_γ of the γ equation as well as the source term $P_{\theta t}$ of the $Re_{\theta t}$ incorporate the empirical transition correlations for natural and bypass transition. Separation induced transition is controlled by

(3)
$$\gamma_{eff} = max(\gamma, \gamma_{sep})$$

with

(4)
$$\gamma_{sep} = min\left(s_1 max\left[0, \frac{Re_\theta}{s_2 Re_{\theta t}} - 1\right] F_{reattach}, 2\right) F_{\theta t}.$$

For the complete description and the definition of the coefficients mentioned in the equations please see Langtry and Menter [4]. Throughout this paper the boundary layers of all no-slip boundaries are highly resolved with a dimensionless wall distance of the wall adjacent cell down to $y^+ = 1$. Convergence was achieved for all cases presented here with density residual drop of at least three orders of magnitude and a relative difference of in- and outlet massflow $\leq 10^{-3}$. Depending on the test case, the convergence of steady simulations was achieved after 2000-4000 iterations.

2.1 Approach Description

There exist several rules of thumb or best practice guides for the prescription of the turbulent length scale, which usually lead to $l_T \approx 10^{-4} m$ for typical turbomachinery conditions. But, this leads to

extremely harsh turbulent decay rates which implies wrong values of turbulent levels and this finally results in a wrong prediction of transitional behaviour on turbomachinery blades. Here, an estimation is derived from the correlation of Baines and Peterson [12]. Originally, this correlation applied to high turbulence flows through screens and reads as follows:

$$Tu = 1.12 \left(\frac{x}{b}\right)^{-\frac{5}{7}} \tag{5}$$

This correlation can be rewritten in terms of turbulent kinetic energy k:

$$\frac{k}{k_0} = \left[\left(\frac{t}{0.06s}\right) + 1\right]^{-\frac{10}{7}} \tag{6}$$

The corresponding specific dissipation rate is:

$$\omega_0 = 220 k_0^{-0.613}. \tag{7}$$

The turbulent length scale estimates after:

$$l_{T,0} = \frac{\sqrt{k_0}}{\omega_0} \tag{8}$$

The T3 ERCOFTAC test series is used to show the effect of different turbulence intensities and varying turbulent length scales on turbulence and transition models. To evaluate the new approach experiments on flat plates from Roach and Brierley [13] are compared to numerical simulations done with and without the new approach.

Case	Tu [%]	Re [10^6]	M_∞ [$-$]	U_∞ [m/s]
T3A	3.0	0.60	0.0154	5.4
T3B	6.0	1.09	0.0282	9.4
T3A-	0.9	2.24	0.0582	19.8

Table 1: Parameter for ERCOFTAC T3-series flat plate

The variation of different values of l_T for the T3B flat plate is shown in figure 1. It is well seen that a variation of l_T results in different rates of turbulent kinetic energy decay. A small value of $l_T = 0.00001m$ predicts a too strong decay, whereas larger values provide a too small dissipation rate. The corresponding impact to the transitional behaviour is shown in figure 2. Here the skin friction coefficient c_f varies very strongly for the different values of l_T.

In figure 1 also experimental data for the normalized turbulent kinetic energy decay $\frac{k}{k_0}$ from the T3 ERCOFTAC test series is shown. It is well seen that the correlation given by Baines and Peterson (B. & P.) after equation 6 reflects the experimental

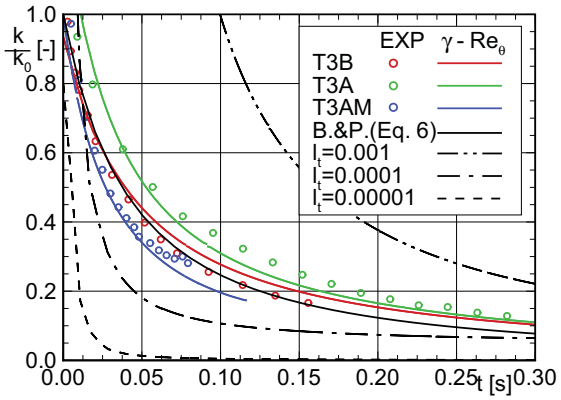

Figure 1: Turbulence decay of T3 flat plate

data in a well appropriate way. Additional TRACE simulations with the new approach for all three test cases are carried out in this figure too. Here also each simulation reproduces the corresponding experimental data very well and the transitional behaviour is predicted correctly for the T3B test case in figure 2. The correct c_f distribution, which is also provided from the numerical simulations with the new approach, is reached for a turbulent length scale of $l_T = 0.001m$. So a prescribed turbulent length scale of $0.001m$ provides a correct decay of turbulent kinetic energy and gives a skin friction coefficient distribution which is accurate enough compared to experimental data.

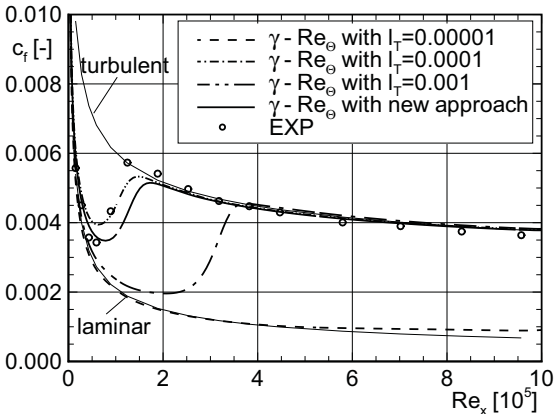

Figure 2: Influence of different l_T on c_f

Besides the flow conditions for transition prediction a reasonably prescribed turbulent length scale of $l_T = 0.001m$ will result in very large value of eddy viscosity for highly turbulent flows (cf. fig. 3). This in turn leads to loss production in high turning flows, e.

g. in the passage between turbine blades. In figure 3 eddy viscosity ratios $\frac{\mu_t}{\mu}$ for the different turbulent length scales are presented. Figure 3 indicates that the loss coefficient ζ also depends on the variation of l_T as higher values of l_T result in higher values of ζ. Obviously, the correct prescription of the turbulent length scale results in improved transition prediction, but also in excessive loss generation in the turbine passage. Both the large value of the turbulence model's diffusive term and the coupling of the production term to the strain is responsible for this loss increase. Since the additional losses are generated above the boundary layer, that means in non-viscous regions, this behaviour is non-physical. For this reason, a criterion for the determination of viscous regions (boundary layers and wakes) has been developed as an additional element of the implemented approach (cf. fig. 4).

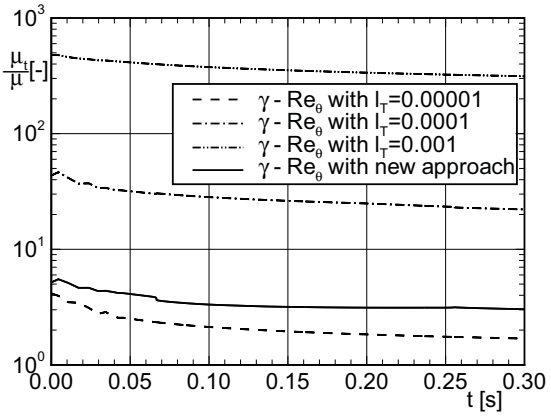

Figure 3: Influence of $l_{T,0}$ on eddy viscosity

This criterion is based on the large values of turbulent dissipation rate ω. It takes the relationship between the turbulent dissipation rate estimated from the k-ω turbulence model and the turbulent dissipation rate in the free stream of the flow estimated by the new approach of Baines and Peterson. The effect of the very high ratio in the boundary layer and wakes is used to separate them from the free stream.

(9) $$\omega_{Quot} = \frac{\omega}{\omega_{FS}}$$

The eddy viscosity is only applied in these viscous regions, effectively preventing the loss production in non-viscous areas by multiplying the eddy viscosity by a factor b_v, which is 1 in the boundary layer and the wake region and near zero in the free stream (cf. fig. 4).

(10) $$\frac{\mu_t}{\mu} := b_v \cdot \frac{\mu_t}{\mu}$$

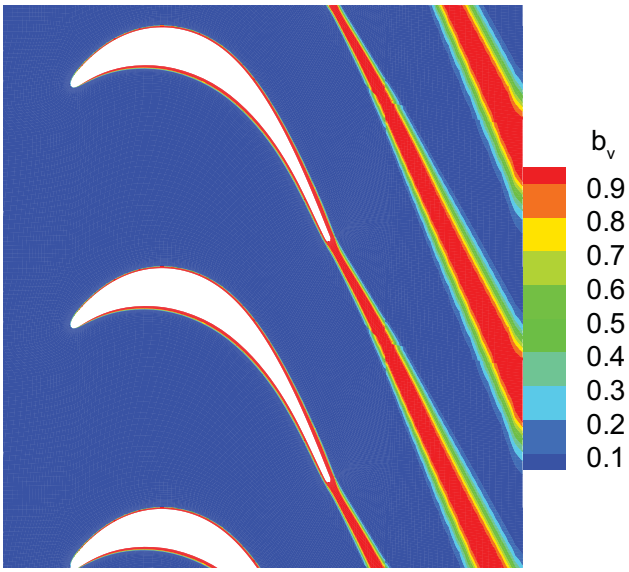

Figure 4: Viscous regions in T106A turbine cascade

As a result, applying the correlation of Baines and Peterson to the TRACE code leads to appropriate turbulence decay rates *and* accurate loss prediction.

Of course, the dissipation rate can also be prescribed according to measured data, if present. If so, the estimation of turbulent length scale by eqs. 7 and 8 is not necessary, but the limitation of eddy viscosity by eq. 10 still can be applied.

As a final step, some minor adaptions to the γ-Re_θ transition model have been conducted, in particular to the separation induced transition formulation at very low Reynolds numbers.

3 TEST CASES

3.1 2D T106A Turbine Cascade

The T106A gives more insight in predicting transition in turbomachinery flow by providing experimental data for varying Reynolds number, also the influence of change in inlet angle and Mach number is shown. A more detailed summary about T106A is given in Hoheisel [14] and Hoheisel [15]. The used mesh consists of 18000 cells and is shown in figure 5.

The dimensionless wall distance of the wall neighboured cells is of the order of $y^+ \approx 1$. The chord length of the profile is about $l = 0.1m$ and the pitch is t_θ=$0.0799m$. The corresponding ratio is $\frac{t_\theta}{l} = 0.799$. For the T106A turbine cascade a large variation of parameters, at a turbulent intensity of $Tu = 4\%$, is conducted, whereas for all investigated parameter just selected cases are shown.

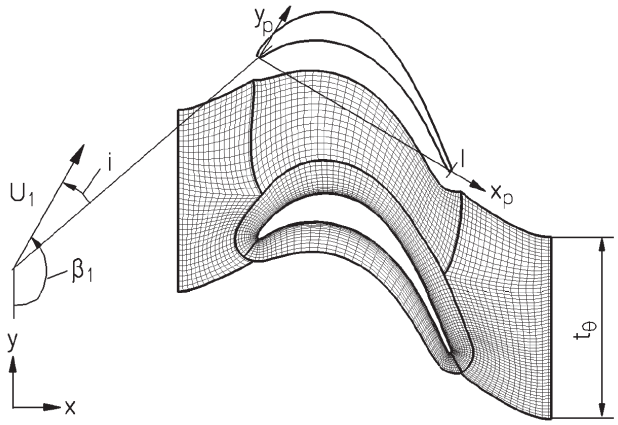

Figure 5: Computational mesh for T106A turbine cascade

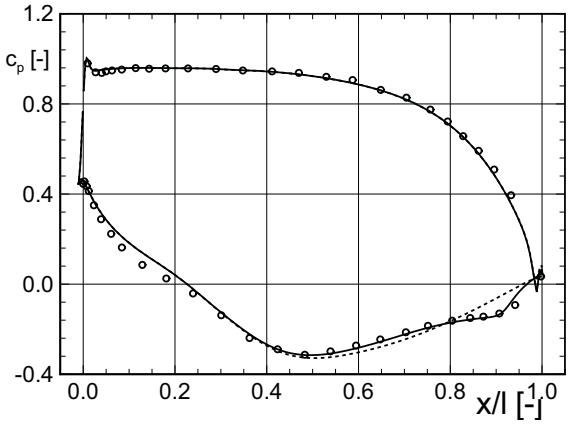

Figure 7: Influence of Reynolds number ($Re_{2th} = 150000$) on pressure coefficient distribution T106A

3.1.1 Reynolds Number

Figure 6 shows the dependency of the loss coefficient on the Reynolds number for a turbulence intensity of $Tu = 4.0\%$. Especially for small values of Re_{2th} a significant rise in loss coefficient is seen, whereas for higher values an almost constant value of ζ can be assumed. The new approach of the transition model can predict both aspects, trend and level, of the Reynolds number influence, whereas the turbulent simulation is able to predict the trend of loss coefficient rise at small values of Reynolds number, but is not able to give the right level of values.

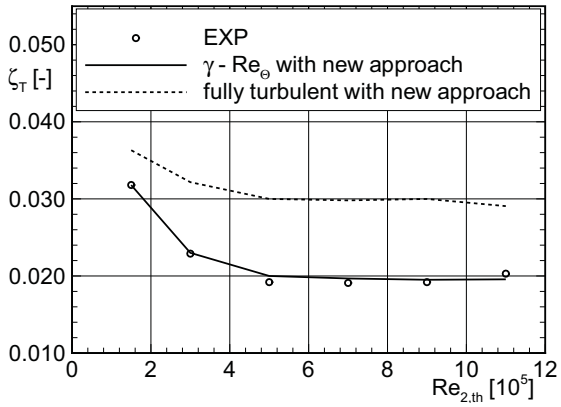

Figure 6: Influence of Reynolds number on loss coefficient T106A

The prediction accuracy of the transition model is also shown for the pressure distribution over the blade surface as seen in the following figures. It is the pressure coefficient distribution c_p given over the true chord length x/l.

The c_p distribution for the smallest given Reynolds number shows a separation bubble at the near of the trailing edge on the suction side of the blade. This separation bubble is well predicted by the transition model. The turbulent simulation is not able to show this transitional behaviour. For higher values of Re_{2th} the size of the separation bubble decreases and finally disappears for $Re_{2th} = 900000$ (not shown).

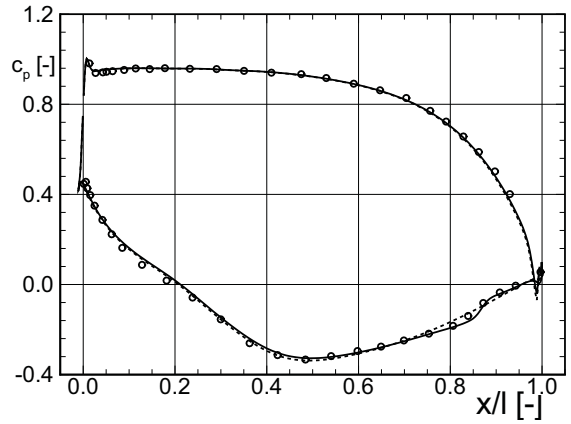

Figure 8: Influence of Reynolds number ($Re_{2th} = 500000$) on pressure coefficient distribution T106A (Design)

3.1.2 Mach Number

As a second influence parameter on the transitional behaviour, the dependency of the loss coefficient on the Mach number is given in fig. 9 (at constant theoretical Reynolds number of $Re_{2th} = 500000$). The transitional simulations are in good agreement with the experiement. Just close to transonic conditions ($M_{2th} \approx 0.955$) the loss coefficient is predicted too high. Also it is seen, that at these transonic con-

ditions ζ of transitional and turbulent simulation are close to each other.

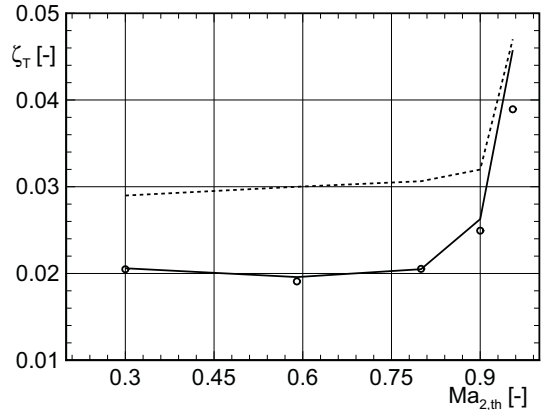

Figure 9: Influence of Mach number on loss coefficient T106A

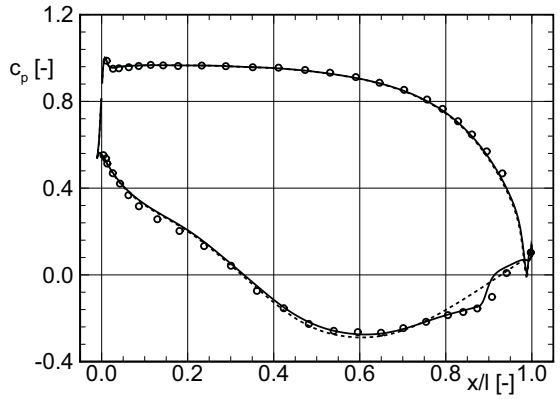

Figure 10: Influence of Mach number $M_{2th} \approx 0.80$ on pressure coefficient T106A

With decreasing Mach number from $M_{2th} \approx 0.955$ the loss coefficient for turbulent flow is considerably overpredicted. Just the trend of decreasing ζ and reaching of an almost constant value is reproduced by the turbulent simulation. This behaviour is also seen in the pressure coefficient c_p distribution. Due to increasing Mach number a separation bubble on the suction side occurs which is very well predicted by the transitional model as seen in figs. 10 and 11. The influence of the Mach number on the pressure side c_p distribution in negligible. The steady acceleration for all Mach numbers investigated here results in a laminar boundary layer for the whole pressure side of the turbine blade. On the suction side of the blade there are significant differences in the pressure coefficient distributions. The most significant change in c_p is the shift of its suction side peak downstream with increasing mach number. The size of the separation bubble is biggest for the highest Mach number and it decreases with decreasing Mach number.

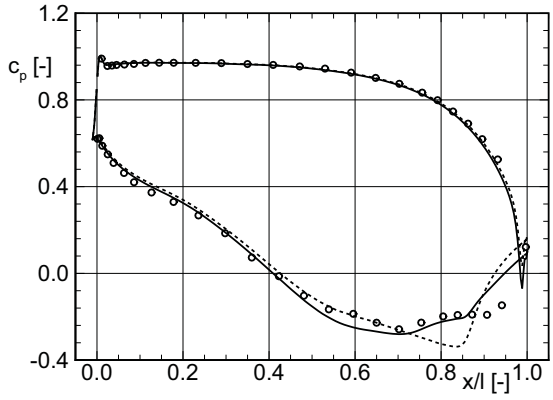

Figure 11: Influence of Mach number $M_{2th} \approx 0.955$ on pressure coefficient T106A

3.1.3 Inlet Angle β_1

As a last influence parameter the inlet angle β_1 was varied. Here different incidence angles of the design inlet angle $\beta_1 = 150.0°$ are shown. Figure 12 shows the dependency of the loss coefficient on the inlet angle.

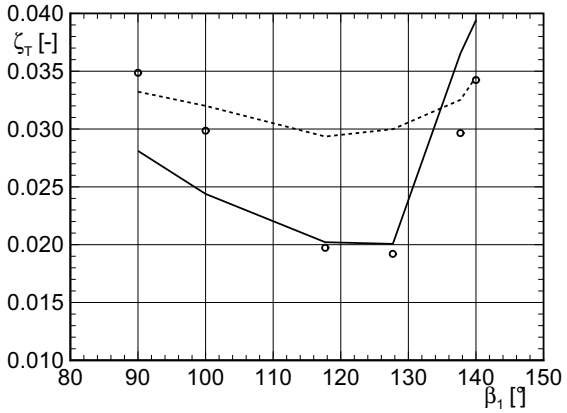

Figure 12: Influence of inlet angle on loss coefficient T106A

As expected, the lowest loss coefficient occurs for the incidence free configuration at design point (β_1=127.7°). The losses are increasing for negative and positive incidence angles. This trend is also predicted by the transitional model, although the values

are not very accurate. The same applies to the turbulent simulation, where the loss values for the highest positive and negative incidence are almost good predicted, but near the design point, they are far away from the experimental data.

As pointed out from the pressure distribution in figure 13 a separation bubble occurs for a large negative incidence angle on the pressure side of the turbine blade due to a leading edge separation. This

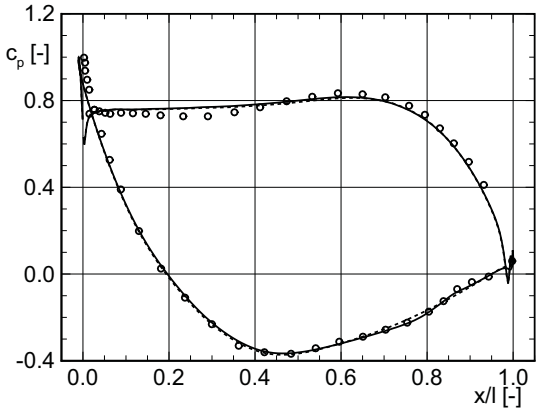

Figure 13: Influence of inlet angle $\beta_1 = 90°$ on pressure coefficient distribution T106A

separation bubble is quite long, starting at about 60% of the axial length of the turbine blade. Downstream of the reattachment point the boundary layer remains in a turbulent state and the acceleration at the rear of the blade does not cause any relaminarization. For

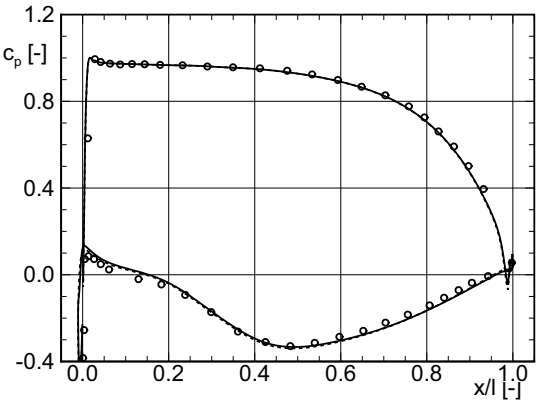

Figure 14: Influence of inlet angle $\beta_1 = 137.7°$ on presure coefficient distribution T106A

the second highest investigated incidence angle a leading edge separation occurs too, which results in a small laminar separation bubble on the suction side of the blade. The whole boundary layer downstream of the transition location remains also in a turbulent state.

Both the transitional and turbulent simulation yield reasonably accurate pressure distributions for both increased and decreased inlet angle, although the corresponding loss predictions show significant errors.

3.2 2D HPA 17/06 Compressor Cascade

In contrast to the previous turbine test case, now the transitional and turbulent simulations are applied to a characteristic compressor test case, the HPA 17/06 compressor cascade. The design and experimental investigation of this compressor cascade have been conducted by the Institute of Propulsion Technology at DLR Cologne, cf. Küsters et al. [16] and Köller [17]. The used computational mesh consists of 10300 cells and is shown in fig. 15. Here, the influence of the Mach number and the inlet angle are investigated.

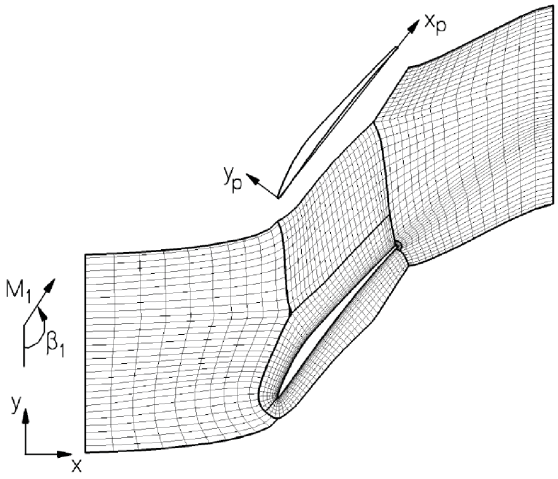

Figure 15: Geometry and computational mesh of HPA 17/06 compressor cascade

3.2.1 Mach Number

In fig. 16 the loss coefficients for different inlet Mach numbers are shown, where only the transitional simulation reasonably reproduces the loss values provided by the experiments. Only for the largest investigated Mach number the loss coefficient was predicted too small for both models.

In the following, isentropic Mach number distributions are presented. They are derived from the static

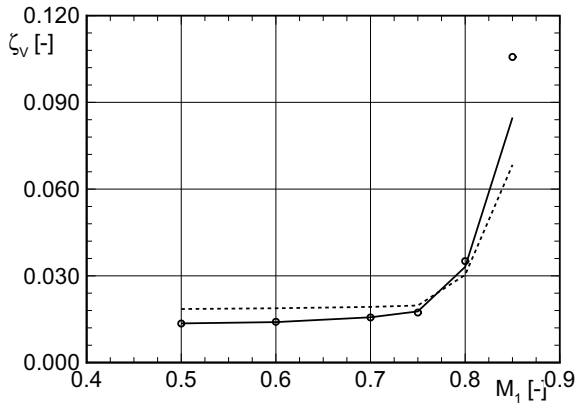

Figure 16: Influence of Mach number on loss coefficient HPA 17/06

pressure distributions as follows:

$$M_{is} = \sqrt{\frac{2}{\kappa - 1}\left[\left(\frac{p_w}{p_{t1}}\right)^{\frac{1-\kappa}{\kappa}} - 1\right]} \tag{11}$$

The results show that the blade loading increases with increasing Mach number as indicated by figs. 17 and 18.

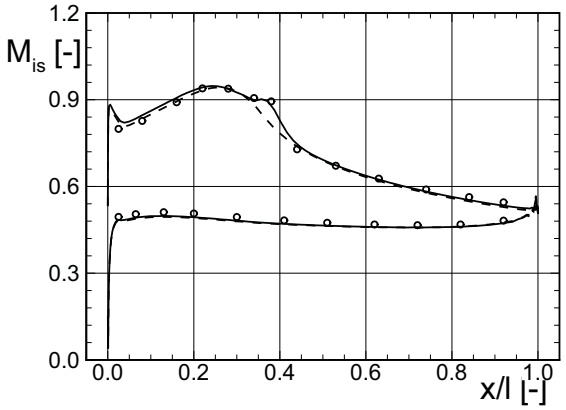

Figure 17: Influence of Mach number $M_1 = 0.70$ (Design) on isentropic Mach number distribution HPA 17/06

Well accepted criteria to evaluate the boundary layer loading are the drop of Mach number on the suction side and the captured area within the Mach number curve. Both are small for the smallest investigated inlet Mach number ($M_1 = 0.50$). This results in small values of loss coefficient as seen in fig. 16. Due to the rise in inlet Mach number the boundary layer loading and the loss coefficient increase. This rise in ζ is small as long as the Mach number distribution on the suction side remains subsonic. At supercritical conditions local supersonic areas with subsequent shock are present, leading to a significant rise in loss coefficient ($M_1 > 0.70$). Besides the separation bubble the transition model is able to predict the distributions of isentropic Mach number more accurately as compared to the turbulent simulations.

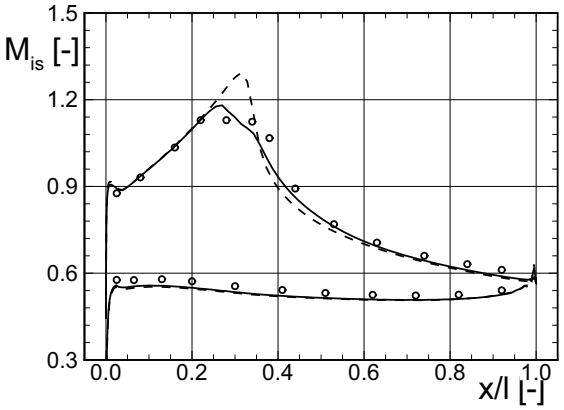

Figure 18: Influence of Mach number $M_1 = 0.80$ on isentropic Mach number distribution HPA 17/06

3.2.2 Inlet Angle

Due to the inlet angle variation, the flow through the cascade results in a rise of loss coefficient for both cases, higher and lower inlet angles, as seen in fig. 19. The higher loss coefficient is a result of higher boundary layer loading on suction and pressure side, for increasing and decreasing incidence, correspondingly. Both the transitional and turbulent simulations capture the loss increase reasonably, but after a closer look, the transitional simulation is more accurate than the turbulent one. Precisely, the loss coefficient of the transitional simulation is in a better agreement with the experiment near the design point (β_1=150.0° and M_1=0.70).

For the lowest inlet angle ($\beta_1 = 142.5°$) a separation bubble on the pressure side is seen in the experimental data. This separation is not predicted by the transition model (cf. fig. 20). On the other hand, the suction side separation downstream the peak is predicted for this and further increasing inlet angles.

For the second highest inlet angle ($\beta_1 = 154.3°$) the laminar-turbulent transition process shifts to the leading edge (cf. fig. 21). This implies a fully turbulent boundary layer on the suction side of the blade. For $x/l > 0.5$ there is a significant difference to the experiments. This is a result of a turbulent separation in the experiment, which has not been predicted by

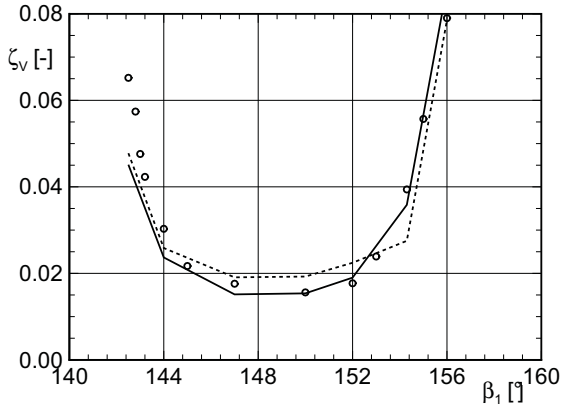

Figure 19: Influence of inlet angle on loss coefficient HPA 17/06

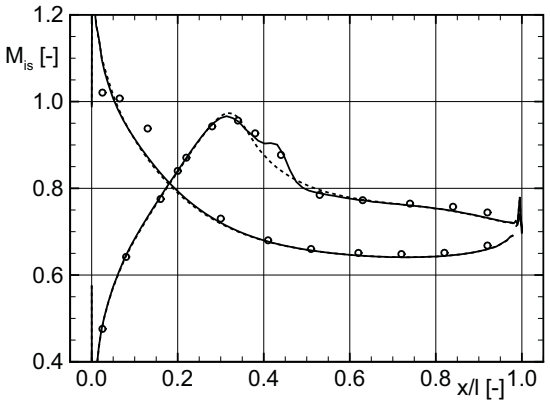

Figure 20: Influence of inlet angle ($\beta_1 = 142.5°$) on isentropic Mach number distribution HPA 17/06

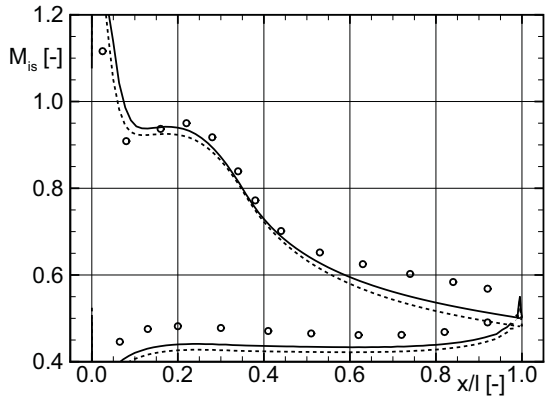

Figure 21: Influence of inlet angle ($\beta_1 = 154.3°$) on isentropic Mach number distribution HPA 17/06

the numerical model. Since the boundary layer is in turbulent state, this is clearly a deficiency of the turbulence model, and not the transition model. Most likely, this behaviour occurs due to the well known separation resistance of the k-ω model. Overall, the prediction accuracy is very good for low and moderate inlet angles, but there are some deficiencies at very high inlet angles.

4 CONCLUSIONS

A correlation for the prescription of the turbulence length scale at inflow boundaries is provided. This correlation aims at high turbulence turbomachinery flows. Furthermore, the free-stream sensitivity of the turbulence model is suppressed by a limitation of eddy viscosity in the non-viscous regions. The method is implemented in a framework of the k-ω two-equation turbulence model and the γ-Re_θ transition model. Three test cases have been investigated: ERCOFTAC T3 flat plate, turbine cascade T106A and compressor cascade HPA 17/06. The influence of Reynolds number, Mach number and inlet angle at the transition location, loss coefficients and pressure distributions is evaluated. Overall, the new approach yields reasonable turbulence dissipation rates and also a very good agreement with the measurements.

ACKNOWLEDGEMENT

The fruitful discussions with our colleague Dr. A. Fiala from MTU Aero Engines are gratefully acknowledged. We also acknowledge our colleagues from DLR Cologne, Institute of Propulsion Technology, for providing the solver TRACE and for their support on numerical issues. The investigations were partly conducted as part of the research programme LUFO-IV/2 - HDV2015. The work was supported by the Bundesministerium für Wirtschaft und Technologie (BMWi) as per resolution of the German Federal Parliament under grant number 20T0806A. The authors gratefully acknowledge MTU Aero Engines for their support and permission to publish this paper. The responsibility for the content lies solely with its authors.

REFERENCES

[1] Mayle, R.E.: *The Role of Laminar-Turbulent Transition in Gas Turbine Engines* Journal of Turbomachinery, Vol. 113, pp. 509-536, October 1991.

[2] Hourmouziadis, J.: *Aerodynamic Design of Low Pressure Turbines* AGARD Lecture Series 167, 1989.

[3] Wilcox, D.C.: *Turbulence Modeling for CFD*, 3^{rd} Edition, DCW Industries, La Canada, 2006.

[4] Langtry, R.B.; Menter, F.R.: *Correlation-Based Transition Modeling for Unstructured Parallelized Computational Fluid Dynamics Codes* AIAA Journal, Vol. 47, No. 12, December, 2009.

[5] Nürnberger, D.: *Implizite Zeitintegration für die Simulation von Turbomaschinenströmungen*, Ph.D. Thesis, Ruhr-Universität Bochum, also DLR Forschungsbericht 2004-27, 2004.

[6] Kügeler, E.: *Numerisches Verfahren zur genauen Analyse der Kühleffektivität filmgekühlter Turbinenschaufeln*, Ph.D. Thesis, Ruhr-Universität Bochum, also DLR Forschungsbericht 2005-11, 2005.

[7] Marciniak, V.; Kügeler, E.; Franke, M.: *Predicting Transition on Low-Pressure Turbine Profiles*, Proc. of V. European Conference on Computational Fluid Dynamics, Lisbon, Portugal, 14.-17. June, 2010.

[8] Becker, K.; Heitkamp, K.; Kügeler, E.: *Recent Progress in a Hybrid-Grid CFD Solver for Turbomachinery Flows*, Proc. of V. European Conference on Computational Fluid Dynamics, Lisbon, Portugal, 14.-17. June, 2010.

[9] Roe, P.: *Approximate Riemann solvers, parameter vector and difference schemes*, J. Comp. Phys., Vol. 34, pp. 357-372, 1981.

[10] Kato, M.; Launder, B.E.: *The Modelling of Turbulent Flow around Stationary and Vibrating Square cylinders*, Proc. 9th Symp. on Turb. Shear Flow, Vol. 9, pp. 10.4.1-10.4.6, Kyoto, Japan, 1981.

[11] Saxer, A.; Giles, M.B.: *Quasi-three-dimensional nonreflecting boundary conditions for Euler equation calculations* AIAA J. Prop. and Power, Vol. 128, pp. 263-271, 1993.

[12] Baines, W.D.; Peterson, E.G.: *An Investigation of Flow through Screens* ASME Paper No. 50-A-23, 1951

[13] Roach, P.E.; Brierley, D.H.: *The Influence of a Turbulent Free-Stream on Zero Pressure Gradient Transition Boundary Layer Development - Part I: Test Cases T3A and T3B* Proc. 1^{st} ERCOFTAC Workshop on Numerical Simulations of Unsteady Flows, Transition and Turbulence, Lausanne, Schweiz, 1990.

[14] Hoheisel, H.: *Entwicklung neuer Entwurfskonzepte für zwei Turbinengitter, Teil 3: Ergebnisse T106* Institutsbericht IB 129-81/26, DFVLR, Braunschweig, 1981.

[15] Hoheisel, H.: *Test Case E/CA-6: subsonic turbine cascade T106* in AGARD- AR-275: Test Cases for Computation of Internal Flows in Aero Engine Components, S. 112-123, Fottner, L. (Ed.), SPS, Loughton, 1990.

[16] Küsters, B.; Steinert, W.; Schreiber, H.A.: *Experimentelle und theoretische Untersuchung des Verdichtergitters KWU-HPA 17/06* DLR IB-325-07-96, 1996.

[17] Köller, U.: *Entwicklung einer fortschritlichen Profilsystematik für stationäre Gasturbinenverdichter* Ph.D Thesis, also DLR Forschungsbericht 1999-20, 2005.